Materials Advances

ROYAL SOCIETY OF CHEMISTRY

PAPER

View Article Online
View Journal | View Issue

Cite this: *Mater. Adv.*, 2024, 5, 5290

A robotic system for automated chemical synthesis of therapeutic agents†

Kai Bao,‡[ab] Jong Seo Yoon,‡[b] Sung Ahn,[a] Jeong Heon Lee,[ab] Conor J. Cross,[b] Myung Yung Jeong,*[bc] John V. Frangioni*[bd] and Hak Soo Choi *[ab]

Received 2nd February 2024,
Accepted 29th April 2024

DOI: 10.1039/d4ma00099d

rsc.li/materials-advances

The development of novel compounds for tissue-specific targeting and imaging is often impeded by a lack of lead compounds and the availability of reliable chemistry. Automated chemical synthesis systems provide a potential solution by enabling reliable, repeated access to large compound libraries for screening. Here we report an integrated solid-phase combinatorial chemistry system created using commercial and customized robots. Our goal is to optimize reaction parameters, such as varying temperature, shaking, microwave irradiation, aspirating and dispensing large-sized solid beads, and handling different washing solvents for separation and purification. This automated system accommodates diverse chemical reactions such as peptide synthesis and conventional coupling reactions. To confirm its functionality and reproducibility, 20 nerve-specific contrast agents for biomedical imaging were systematically and repeatedly synthesized and compared to other nerve-targeted agents using molecular fingerprinting and Uniform Manifold Approximation and Projection, which lays the foundation for creating reliable and reproductive chemical libraries in bioimaging and nanomedicine.

Introduction

Automated synthesis, leveraging robotics, computer-controlled systems, and advanced instrumentation, represents an innovative approach to chemical synthesis that has undergone notable advancements in recent years, reshaping the landscape of chemistry.[1–3] Automated synthesis encompasses various methodologies, such as parallel synthesis, flow chemistry, and microfluidics, each offering distinct advantages in efficiency, scalability, and flexibility. For example, pioneering work in flow chemistry, coupled with automation, enables precise control over reaction parameters, thereby facilitating the synthesis of complex molecules like small molecules, oligonucleotides, and peptides with improved yields and purity.[1–5] Furthermore, the development of packed-beds, modular cartridges, photochemical reactors, plasma reactors, catalytic membrane reactors, and electrochemical reactors by various renowned laboratories has emerged as a result of discoveries in flow chemistry, further advancing progress in this field.[3,6–10]

Recent advancements in robotics technology, computer science, and artificial intelligence have significantly accelerated life science research in both academic institutions and industry.[11–14] Many automated synthesis systems have been developed for synthesizing therapeutic and clinical agents with minimal human intervention.[15–17] For synthesizing a large chemical library, solid-bead-based combinatorial chemistry is a viable option for automated high-throughput synthesis and screening.[18–20] In particular, one-bead one-compound (OBOC) libraries have become a powerful tool in the process of lead compounds discovery because of the high structural diversity obtained by the split-and-pool method.[21–26] When automated synthesis is designed for combinatorial libraries, they can be used to produce many new compounds, which are then subsequently available for drug candidates discovery by high-throughput screening.[27–30] Thus far, several OBOC-based combinatorial libraries have been reported to solve the large demand for new drug candidates. However, reproducible and controlled sequential synthesis has been a major challenge in this field.[31–34] Therefore, there is a need to develop a simple, versatile automated system for combinatorial peptide synthesis and other conventional chemical conditions to address these challenges and facilitate drug candidate discovery through high-throughput screening.

Nerve-targeting contrast agents are important because nerve damage during surgery is a major cause of morbidity.[35] Even for experienced clinicians, nerve-sparing surgery is a major challenge and surgical nerve damage leads to chronic pain as well as loss of function and decreased quality of life.[36–39]

[a] *Gordon Center for Medical Imaging, Department of Radiology, Massachusetts General Hospital and Harvard Medical School, Boston, MA 02114, USA. E-mail: hchoi12@mgh.harvard.edu*
[b] *Center for Molecular Imaging, Department of Medicine, Beth Israel Deaconess Medical Center, Boston, MA 02215, USA*
[c] *Department of Cogno-Mechatronics Engineering, Pusan National University, Busan 46241, South Korea. E-mail: myjeong@pusan.ac.kr*
[d] *Curadel, LLC, Natick, MA 01760, USA. E-mail: jvfrangioni@curadel.com*
† Electronic supplementary information (ESI) available. See DOI: https://doi.org/10.1039/d4ma00099d
‡ These authors contributed equally to this work.

Therefore, it is imperative to develop nerve-targeting contrast agents for accurately tracking nerves and preserving them during intraoperative procedures.[40]

In this study, we developed an integrated chemistry system and demonstrated its utility in the automated synthesis of nerve-targeting contrast agents. Compared to existing automated systems, our robotic chemistry system offers several distinct capabilities (Table S1, ESI†): (1) execution of conventional chemical reactions spanning a range of temperatures, agitation levels, and microwave conditions; (2) manipulation of large-sized solid beads through aspiration and dispensing; (3) automated capping and decapping processes; and (4) management of six different washing solvents and waste disposal. Leveraging conventional robotic technologies, we amalgamated these essential chemistry functions into a single sequential automated system, devised the requisite software to oversee the entire process, and subsequently verified the sequential functionalities for synthesizing nerve-specific contrast agents.

Results and discussion

Integration of five functional robots

As depicted in Fig. 1, the robotic chemistry system is composed of five main functional robots including a 360° Robot Arm (RA), a Capper–Decapper (CAP), a Split-Pool Bead Dispenser (SPBD), a Liquid Handler (LH) with the heating/cooling rack (Fig. S1, ESI†), and a Microwave Reactor (MWR). All combined robots perform functional roles with customized software to achieve automated solid-based chemistry. The detailed role of each robotic system is described in ESI.†

Integration of software

The computer software controls the whole system through RS-232 serial binary single-ended data ports. Software gives commands to each robotic system by reading a command sequence, which the user can create using the dialog box of the command sequence creator (Fig. 2).

As shown in Fig. 2(A), the automated graphical user interface (GUI) is the main interface for the software. A series of command sequences are used to drive the robotic system to achieve automated syntheses. In addition, to further reduce the workload of the user, a GUI for the command sequence creator software is developed for the creation and easy access of a command sequence for the synthesis (Fig. 2(B) and (C)). Each user can write a command sequence in a text file and then load it into the automated chemistry software to run serial syntheses.

Automated synthesis for nerve-targeting agents

Previously, we have conducted the structure–activity relationship of nerve-highlighting fluorophores, and more than 200 analogues of the lead compound 4,4′-[(1*E*,1′*E*)-(2-methoxy-1,4-phenylene)bis(ethene-2,1-diyl)]dianiline (BMB) have been manually synthesized over 2 years.[41] We believe that parallel or combinatorial syntheses of small-molecule libraries will significantly facilitate and reduce the time taken in the development of such ligands.[32–34]

To access the functional features of the automated robotic chemistry system, a parallel synthesis of the BMB library including 20 analogues was attempted (Fig. 3(A)). Fig. S2 (ESI†) lists the command sequence for the automated synthesis of the

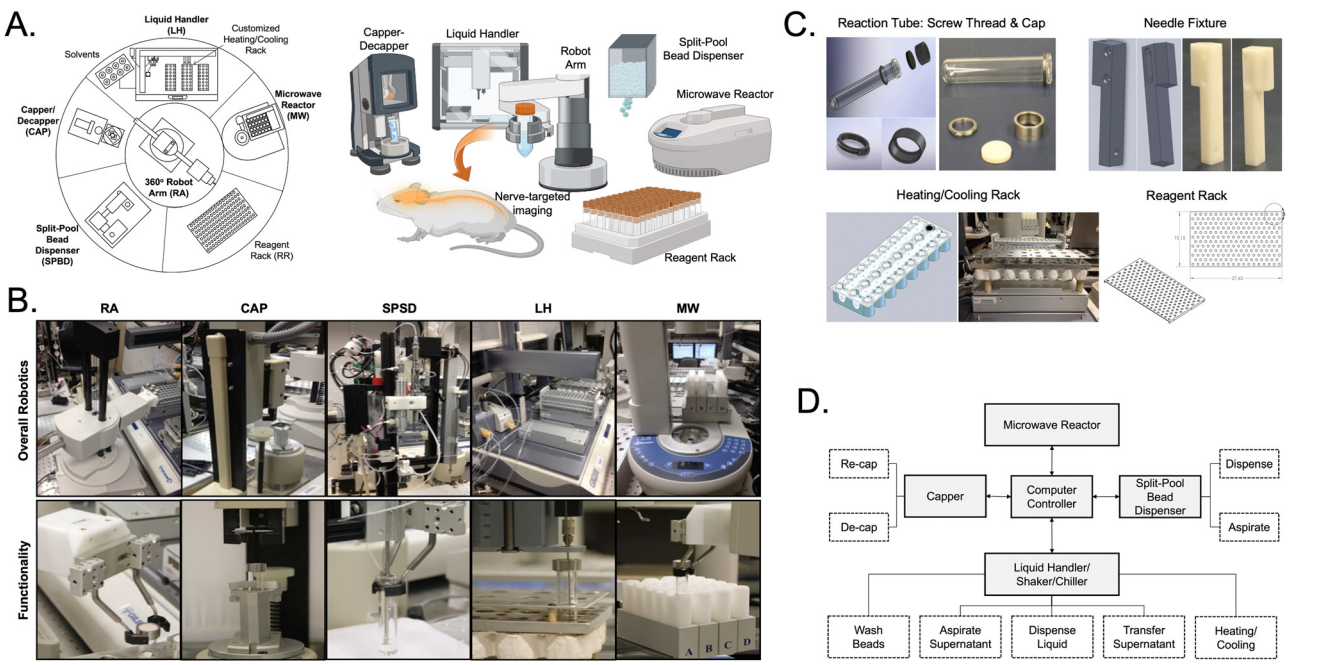

Fig. 1 Overall design and functionality of the automated chemistry system: (A) schematic and (B) gross picture of the combined robotic system. All five components are placed around the 360° Robot Arm. (C) Customized heating & cooling rack, and customized tube and screw cap which allows facile and repeatable opening or closing. (D) General workflow and functionality of the robotic chemistry system.

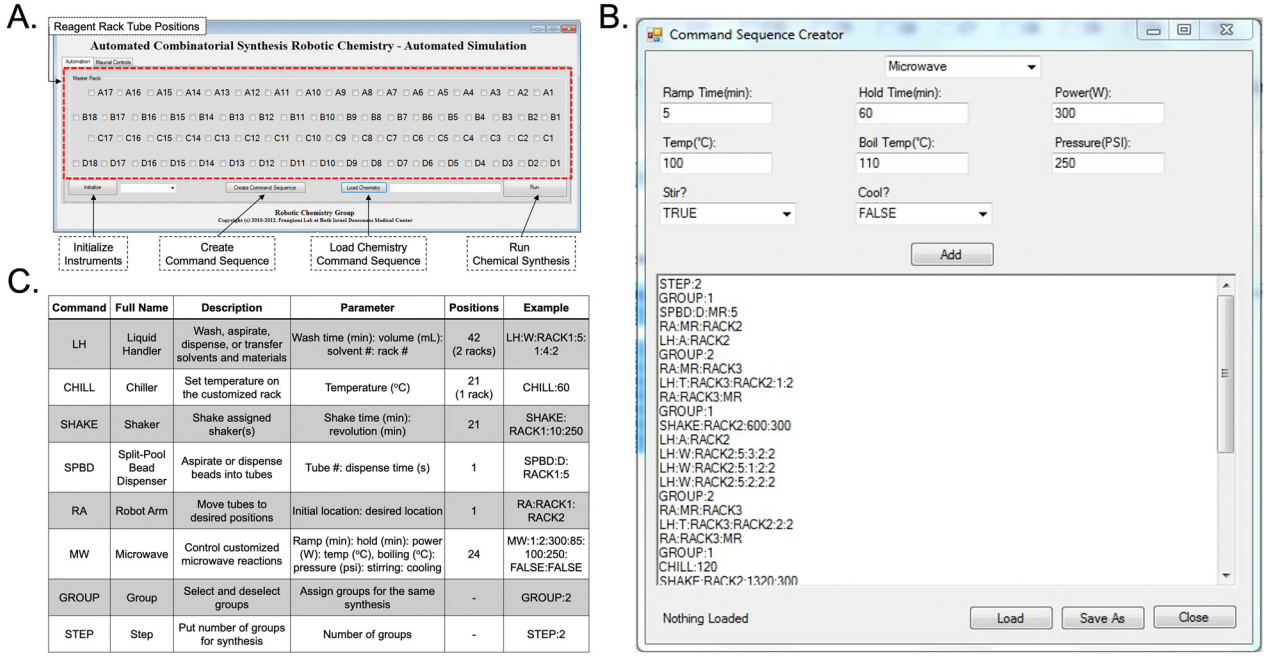

C.

Command	Full Name	Description	Parameter	Positions	Example
LH	Liquid Handler	Wash, aspirate, dispense, or transfer solvents and materials	Wash time (min): volume (mL): solvent #: rack #	42 (2 racks)	LH:W:RACK1:5:1:4:2
CHILL	Chiller	Set temperature on the customized rack	Temperature (°C)	21 (1 rack)	CHILL:60
SHAKE	Shaker	Shake assigned shaker(s)	Shake time (min): revolution (min)	21	SHAKE:RACK1:10:250
SPBD	Split-Pool Bead Dispenser	Aspirate or dispense beads into tubes	Tube #: dispense time (s)	1	SPBD:D:RACK1:5
RA	Robot Arm	Move tubes to desired positions	Initial location: desired location	1	RA:RACK1:RACK2
MW	Microwave	Control customized microwave reactions	Ramp (min): hold (min): power (W): temp (°C), boiling (°C): pressure (psi): stirring: cooling	24	MW:1:2:300:85:100:250:FALSE:FALSE
GROUP	Group	Select and deselect groups	Assign groups for the same synthesis	-	GROUP:2
STEP	Step	Put number of groups for synthesis	Number of groups	-	STEP:2

Fig. 2 Software design and command sequence for the automated chemistry system: (A) Graphical user interface (GUI) includes ⟨Initialize⟩, ⟨Create Command Sequence⟩, ⟨Load Chemistry⟩, and ⟨Run⟩ buttons to run a sequential combinatorial synthesis. (B) The Command Sequence Creator functions to create a command sequence for the automated chemistry system. (C) The command sequence table describes functions and parameters of each command. Shown are examples of each command, parameter, and position in each system to be executed.

BMB library. The whole process includes dispensing beads, transferring tubes and reagents/reactants, washing, and shaking beads, and moving around tubes. Chemical reactions are designed to perform either under heat or microwave conditions. As shown in Fig. 3(B), the first step for the automated synthesis is the loading of 4-vinylaniline (block 1, Fig. S3 and S4, ESI†) onto the 2-chlorotrityl resin in 1 mL of DCM containing 80 μL of DIPEA. The Heck reaction of compound **1** with block 2 catalysed by $Pd(OAc)_2/P(O\text{-}Tol)_3$/TBAB at 100 °C afforded the corresponding substituted alkenes **2**, which were treated with KOtBu in toluene under microwave conditions to furnish compound **3**. Finally, the target compounds were cleaved from beads using 20% TFA/DCM, which were characterized by ultra high-pressure liquid chromatography (UPLC; Fig. S5 and S6, ESI†) and matrix-assisted laser desorption/ionization time-of-flight mass spectrometry (MALDI-TOF MS, Table S2, ESI†). To test the reliability and reproducibility of the automated system, 20 BMB derivatives were synthesized three times, and the result was compared with that obtained by manual synthesis (Table 1 and Fig. 3(C)). In total, the entire BMB library could be automatically synthesized within 72 h, which was significantly less than the same scale manually parallel synthesis (120 h). All the 20 library members are obtained with an average overall yield of 29% and an average library purity of 51%, with greater than 70% purity for 7 compounds (Fig. S6, ESI†).

Scaled-up synthesis of compounds to support the subsequent stages of preclinical *in vivo* testing is often a difficult task in pharmaceutical research.[42] After testing the reproducibility of our automated system, we selected compounds from 3 different groups (compounds **1**, **4**, and **9**) to confirm the yield and purity of large batch synthesis. These three compounds were chosen for the scale-up synthesis due to the following reasons: (1) compound **9** is BMB, the positive control for the following bioassays; (2) the synthesis of compound **9** featured the use of a *tert*-butyloxycarbonyl (BOC) as the protecting group; (3) compounds **1** and **4** were found to show similar or brighter nerve fluorescence compared to BMB in our previous study;[41] and (4) the *p*-substituent groups of the right side benzene ring included electron withdrawing/donating groups. Since it is known that the biodistribution and targeting patterns of small molecule agents are predominantly governed by the overall molecular charges, lipophilicity, and polarity, we compared these **3** compounds for further *ex vivo* and *in vivo* evaluations (Table 2).

Large-batch synthesis is performed by adding beads in an excess of 5-fold (50 mg) in a tube with the same command sequences as those in small-scale synthesis. The final yield of compounds **1**, **4**, and **9** is 55% (12 mg, purity 92%), 51% (14 mg, purity 93%), and 20% (5 mg, purity 34%), respectively (Table 1). These results are comparable to or even greater than those obtained from manual syntheses, where purity for compounds **1**, **4**, and **9** was 69.8%, 48.6%, and 69.6%, respectively.[41]

Ex vivo nerve targeting assay

While the detailed mechanism remains not fully understood, speculative evidence suggests that myelin basic protein (MBP) may serve as the binding target for the designed compounds.[43] Additionally, physicochemical properties such as log *D*, topological polar surface area (TPSA), the sum of hydrogen bond

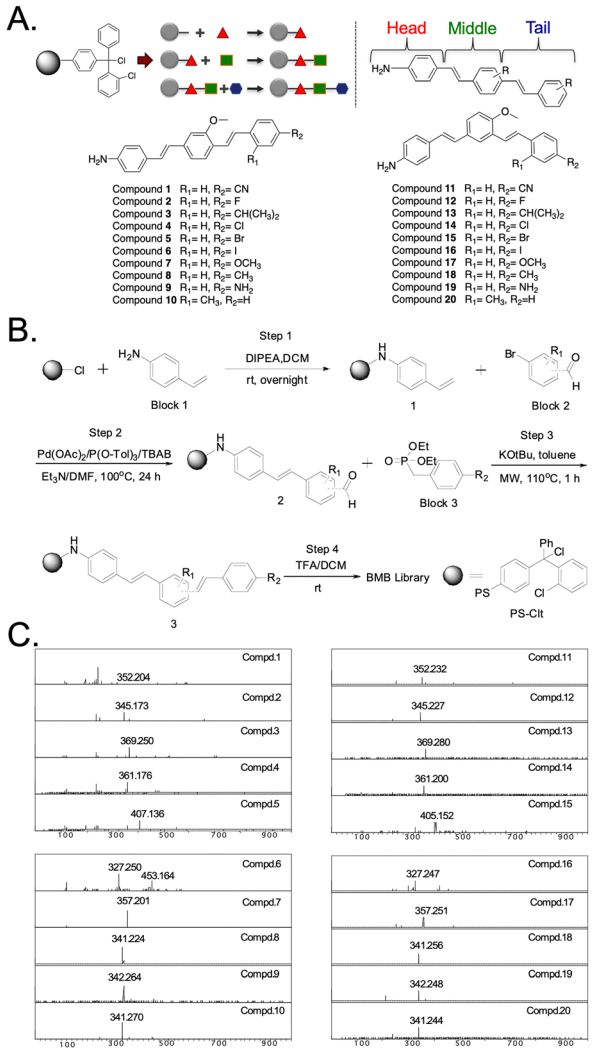

Fig. 3 Automated synthesis of nerve-specific contrast agents: (A) chemical structures of nerve-targeting fluorescent agents (20 BMB analogues). (B) Solid-phase synthetic route of BMB library. Chloro-(2′-chloro)trityl polystyrene resins with a diameter of 400–450 μm were used (capacity = 1.19 mmol g^{-1}). (C) MALDI-TOF mass spectra of each target compound. 2,5-Dihydroxybenzoic acid (DHB) was used as the matrix for ionization.

Table 1 Purity and yield comparison of automated synthesis *vs.* manual synthesis[a]

	Automated small batch (10 mg resins)		Manual synthesis (10 mg resins)		Automated large batch (50 mg resins)	
Time[b]	72 h		120 h		46 h	
#	Purity (%)	Yield (%)	Purity (%)	Yield (%)	Purity (%)	Yield (%)
1	68 ± 11	36	92	56	92	55
2	20 ± 2	19	93	51	N.D.	N.D.
3	16 ± 4	N.D.	95	60	N.D.	N.D.
4	92 ± 6	41	98	62	93	51
5	81 ± 2	32	98	58	N.D.	N.D.
6	90 ± 1	34	66	44	N.D.	N.D.
7	<10	N.D.	<10	N.D.	N.D.	N.D.
8	71 ± 1	25	60	23	N.D.	N.D.
9	49 ± 6	23	36	20	34	20
10	86 ± 3	36	13	ND	N.D.	N.D.
11	78 ± 8	27	94	49	N.D.	N.D.
12	33 ± 3	36	96	40	N.D.	N.D.
13	46 ± 9	30	94	54	N.D.	N.D.
14	76 ± 5	39	94	64	N.D.	N.D.
15	20 ± 2	12	96	50	N.D.	N.D.
16	70 ± 4	27	82	36	N.D.	N.D.
17	14 ± 1	N.D.	68	47	N.D.	N.D.
18	30 ± 2	24	88	55	N.D.	N.D.
19	22 ± 2	18	23	14	N.D.	N.D.
20	38 ± 3	30	93	62	N.D.	N.D.
M ± SD	51 ± 29	29 ± 8	74 ± 30	47 ± 15	73 ± 34	42 ± 19

[a] Purity was calculated based on the integrations of the UPLC band on ELSD, HPLC yields of automated small batch and manual synthesis were obtained by using compound **9** as the standard (Fig. S5 and S6, ESI). For compounds obtained through the automated small batch synthesis, purities were obtained from three independent experiments (mean ± SD). N.D. = not done. [b] Timescales (h) for steps in the workflow.

Table 2 Physicochemical properties of nerve-specific compounds[a]

Compd	M_W (Da)	log *D*, pH 7.4	TPSA (Å^2)	Rotatable bonds	H-bond acceptors	H-bond donors
1	352.44	5.52	59.04	5	3	1
4	361.87	6.27	35.25	5	2	1
9	342.44	4.84	61.27	5	3	2

[a] Physicochemical properties including distribution coefficient (log *D* at pH 7.4), topological polar surface area (TPSA), rotatable bonds, and H-bond acceptors/donors were calculated by MarvinSketch 16.12.12 (ChemAxon).

acceptors and donors, as well as the number of rotatable bonds, are pivotal for effective nerve targeting.[44] To confirm the functionality of nerve targeting agents synthesized automatically using robots, we used compounds **1**, **4**, and **9** for *ex vivo* nerve-specific fluorescence assay. The compounds were purified by preparative TLC (35%, 31%, and 14% isolated yields, respectively) prior to biological evaluations and their purity was confirmed by ^{1}H-NMR spectroscopy (Fig. S7–S9, ESI†). Prior to tissue binding test, we compared the brightness of compounds **1**, **4**, and **9** in test tubes by dissolving the pure powder in DMSO, 5% dextrose solution (D5W) containing 5% Cremophor (C-D5W), or FBS at a concentration of 100 μM (Fig. S10, ESI†). Compounds **1** and **4** showed reasonably high brightness in all three solutions compared with compound **9**. Next, we incubated pig sciatic nerve cut in cross section with 100 μM each fluorophore formulated with C-D5W as previously reported, and their images were taken using a Nikon TE2000 microscope.[41]

As shown in Fig. 4(A), all **3** fluorophores exhibited strong fluorescence signal throughout the cross-sectioned nerve fascicle because of high lipophilicity (high log *D* values > 4.5). Interestingly, compounds **1** and **9** (BMB; positive control) displayed a similar level of background signals in epineurium and adipose tissues, which lowered the overall signal-to-background ratio (SBR) of nerve fascicle against adipose tissue. On the other hand, compound **4** showed high nerve-specific uptake and retention in the fascicle and negligible uptake in the surrounding adipose tissue (SBR > 3.0), which may be

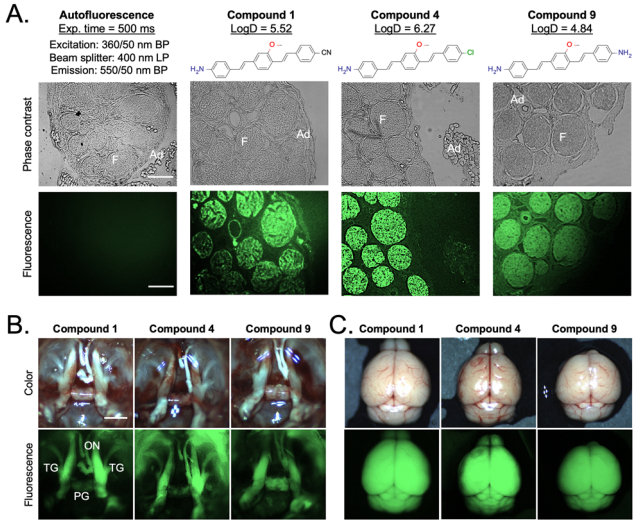

Fig. 4 Nerve-targeting assay for BMB derivatives obtained from automated synthesis. (A) *In vitro* nerve-targeting assay. Nerve-specific fluorescence intensity was determined using staining of pig sciatic nerve cut in cross section and incubated with 100 μM of **3** representative compounds. Control autofluorescence images with equivalent exposure time and filter information are shown. F = nerve fascicle; Ad = adipose. Scale bars = 200 μm. (B) and (C) *In vivo* nervous tissue targeting using compounds **1**, **4**, and **9**. 0.5 mg kg^{-1} of each compound in D5W was injected intravenously into CD-1 mice 4 h prior to imaging. All images were acquired from (B) trigeminal ganglia and optic nerve, and (C) intact brain tissue by intraoperative fluorescence imaging system. ON = optic nerve; TG = trigeminal ganglia; PG = pituitary gland. All fluorescence images have identical exposure times and normalizations. Scale bars = 25 mm.

caused by its high log *D* at pH 7.4 (6.27) with relatively low TPSA (35.25) as depicted in Table 2.[40,41]

In vivo nerve imaging

Next, we explored *in vivo* imaging of nervous tissue using the **3** compounds showing high *ex vivo* nerve tissue binding. Each compound (0.5 mg kg^{-1} dose in IV formulation) was injected intravenously into 25 g CD-1 mice to confirm the *in vivo* uptake in central and peripheral nervous systems.[45] We sacrificed the fluorophore-injected mice 4 h post-injection and exposed trigeminal ganglia, optic nerve, and brain under the intraoperative fluorescence imaging system (Fig. 4(B), (C) and Fig. S11, ESI†). All neural tissues were highlighted with expressing strong fluorescence intensity, which is a strong evidence of blood–brain barrier permeability as previously reported.[41] Although compound **4** showed relatively lower signals in trigeminal ganglia due to the metabolic behaviour of chlorinated substituent, the signals in peripheral nerves were significantly higher ($^*P < 0.05$) than the other two compounds (Fig. S11, ESI†).

UMAP data analysis

To understand the nerve targeting of compounds **1**, **4**, and **9**, we performed high-dimensional data analysis of their structures. We first used a common featurization method for deep learning of chemical databases, the Morgan fingerprint,[46] to process all 250 compounds (the 20 BMB analogues appended to the 230 compounds in our previous study).[41] This allows for structural comparisons through dimension reduction techniques, such as the Uniform Manifold Approximation and Projection (UMAP).[47]

Using the plots generated through the UMAP and plotting the compounds, the entire library of 250 compounds formed several clusters, based on the similarity of the molecules. Each point corresponding to the 230 compounds was coloured by their performance, with a darker colour meaning higher performance. As shown in Fig. 5, compounds **1–10** and compounds **11–20** naturally separated, with compounds **1–10** residing in a cluster of generally higher performance. Also using the UMAP coordinate data, we compiled a table of the number of high-performing compounds near to each of our 20 compounds. Comparing this with our UMAP plot, it was found that while compounds **2**, **6**, and **7** were near the margin of the cluster, compounds **1**, **4**, and **9**, resided closer to the centre, which indicates a deeper similarity with the high-performing compounds.

Traditional manual synthesis in the solution phase is labour-intensive, prone to human error, time-consuming, and can result in sample loss.[48,49] Although solid-based OBOC chemistry offers a more consistent and reliable approach, most chemical libraries are established by manual synthesis as automated robotic systems are complex and expensive.[50] This hurdle is overcome by the integration of commercial and custom robotics with custom software. Compared to that of manual synthesis, the use of an automated robotic system permitted the synthesis of all target compounds while maintaining similar purity and yield. On the other hand, robotic chemistry systems in life science lag their industrial and

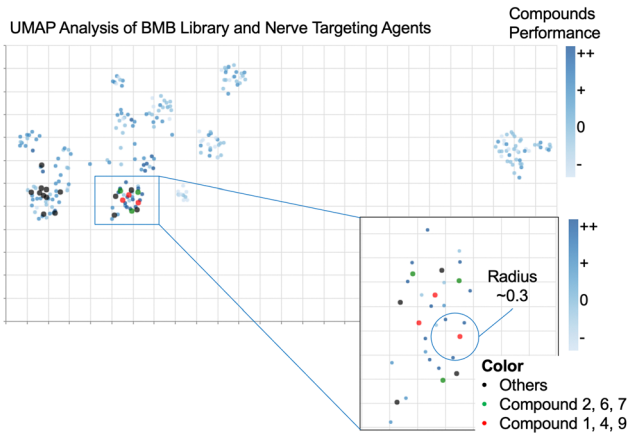

Compound	1	2	3	4	5	6	7	8	9	10	11	12	13	14	15	16	17	18	19	20
# Nearest Neighbors	2	2	1	2	0	3	2	1	3	0	0	0	1	0	0	0	0	0	0	1

Fig. 5 UMAP plot of the BMB compound library and the number of nearest high-performing neighbours for the **20** compounds. Each compound from the previous study uses the following quantitative scale: – = nerve fluorescence equivalent to control autofluorescence; 0 = nerve fluorescence lower than BMB, but higher than control autofluorescence; + = nerve fluorescence equivalent to BMB with the same exposure time; and ++ = nerve fluorescence brighter than BMB with lower exposure time required for imaging.

clinical counterparts due to an array of inhibiting factors, including financial and spatial constraints, as well as the flexibilities of the automatic system. From this perspective, development of bespoke laboratory automation, and repurposing existing equipment, seems an important resource for those choosing this route to automation.[12]

Nevertheless, the developed system in this study has room for improvement. First, the size of beads is critical for furnishing high quantity with high purity. To achieve this goal, 400–450 μm CTC polystyrene resins are selected, where the maximum loading capacity of beads is 1.19 mmol g^{-1}, while conventional size of beads is less than 200 μm. Second, washing steps need to be improved. Although an extensive washing process (three different solvents, 5 mL × 3 times) is applied, after the Heck reaction, the residual reactants (*e.g.*, Pd catalyst) adsorbed on the bead surface are very difficult to eliminate by automatic washing. These residual reactants block the following Wittig reactions with block 3. Third, an anhydrous reaction environment needs to be considered. Most commercially available resins for OBOC, such as CTC beads, are sensitive to moisture, but our robotic chemistry system cannot provide a perfectly sealed environment. At the start of the synthesis, if the beads remain in a very long duration (more than 3 h) in DMSO in the bead dispenser, the small portion of water contained in DMSO decreases the chemical reactivity, thereby resulting in a lower yield. However, if the beads are exposed to anhydrous DMSO and are dispensed within 1 h, the average purity of the final product increases up to 51% as compared with that using 99% DMSO with a longer duration up to 4 h (32% purity). Finally, we used special beads to prove the success of our custom robotic systems as well as the software design and command sequences, although many other OBOC combinatorial strategies have been used extensively in drug candidates discovery during the past decades.[21,22]

Automated robotic flow platforms in chemical synthesis received wide attention in recent years, while solid-phase combinatorial chemistry including compound library development and high throughput bio-evaluations, are still the important components of modern drug development.[51] OBOC library strategy holds the greatest potential for the rapid identification of novel hits against emerging drug target. However, further developments are still needed to expand the utility of the OBOC method to non-peptide chemical scaffolds, as the tentative explorations in this work.

The compound amount and complexity in our current work is limited. Here, our goal is to confirm the functionality and reproducibility of the automated chemistry system, by performing conventional chemical reaction conditions. We will continue to optimize our robots combined with the OBOC strategy in the development of fluorophore libraries with more quantity and structural complexity, and high throughput biomedical evaluations which have been described by our group.[18,31]

Conclusions

In summary, we successfully developed a new automated chemistry system combining commercially available and customized robots. We also created integrated software to operate all the robots. The results demonstrate that solid-phase automation accommodates diverse chemical reactions. Moreover, we executed automated syntheses for a BMB library three times to confirm the reproducibility for creating reliable small-molecule libraries. Finally, the selected compounds **1**, **4**, and **9** were scaled up to the 5-fold level to demonstrate the capability for large-batch syntheses. As compared to laboratory-scale manual synthesis, automated chemistry synthesis formed all target compounds, and large-batch syntheses gave reproducible yield and purity, which were confirmed by *ex vivo* and *in vivo* nerve targeting assays.

As technology advances, more and more complex chemical processes, and even whole workflows such as library preparation or liquid handling, can be automated. State-of-art automatic synthetic systems are expected to continually appear in more laboratories. A single piece of equipment, such as an automated pipetting system or automatic liquid and/or solid dispenser, or a fully automated workflow can be a gamechanger for the laboratories utilizing them. We believe that our work is meaningful in inspiring people in academia and industry to try the concepts, experiments, or skills within the broad term of combinatorial chemistry and automation. Applications of this automated system for the solid-phase synthesis of other small-molecule libraries are currently underway.

Author contributions

KB, JSY, SA, JHL, and CJC performed the experiments. KB, JSY, MYJ, JVF, and HSC reviewed, analysed, and interpreted the data, and KB, JSY, JHL, MYJ, JVF and HSC wrote the paper. All authors discussed the results and commented on the manuscript.

Conflicts of interest

There are no conflicts to declare.

Acknowledgements

We thank Dr Yangsun Kim (HST, Newark, NJ, USA) for technical and financial support. This study was supported by the following grants: NIH/NCI #R01CA115296 and #R01CA280968, and the Nehemias Gorin Foundation. The content expressed is solely the responsibility of the authors and does not necessarily represent the official views of the NIH.

Notes and references

1 B. Burger, P. M. Maffettone, V. V. Gusev, C. M. Aitchison, Y. Bai, X. Wang, X. Li, B. M. Alston, B. Li, R. Clowes, N. Rankin, B. Harris, R. S. Sprick and A. I. Cooper, *Nature*, 2020, **583**, 237–241.
2 C. W. Coley, D. A. Thomas, J. A. M. Lummiss, J. N. Jaworski, C. P. Breen, V. Schultz, T. Hart, J. S. Fishman, L. Rogers,

H. Gao, R. W. Hicklin, P. P. Plehiers, J. Byington, J. S. Piotti, W. H. Green, A. J. Hart, T. F. Jamison and K. F. Jensen, *Science*, 2019, **365**, eaax1566.
3 A. Adamo, R. L. Beingessner, M. Behnam, J. Chen, T. F. Jamison, K. F. Jensen, J.-C. M. Monbaliu, A. S. Myerson, E. M. Revalor, D. R. Snead, T. Stelzer, N. Weeranoppanant, S. Y. Wong and P. Zhang, *Science*, 2016, **352**, 61–67.
4 M. Guberman and P. H. Seeberger, *J. Am. Chem. Soc.*, 2019, **141**, 5581–5592.
5 A. J. Mijalis, D. A. Thomas, M. D. Simon, A. Adamo, R. Beaumont, K. F. Jensen and B. L. Pentelute, *Nat. Chem. Biol.*, 2017, **13**, 464–466.
6 C. Yang, A. R. Teixeira, Y. Shi, S. C. Born, H. Lin, Y. Li Song, B. Martin, B. Schenkel, M. Peer Lachegurabi and K. F. Jensen, *Green Chem.*, 2018, **20**, 886–893.
7 J. Wengler, S. Ognier, M. Zhang, E. Levernier, C. Guyon, C. Ollivier, L. Fensterbank and M. Tatoulian, *React. Chem. Eng.*, 2018, **3**, 930–941.
8 G. Laudadio, W. de Smet, L. Struik, Y. Cao and T. Noël, *J. Flow Chem.*, 2018, **8**, 157–165.
9 E. G. Moschetta, S. Negretti, K. M. Chepiga, N. A. Brunelli, Y. Labreche, Y. Feng, F. Rezaei, R. P. Lively, W. J. Koros, H. M. L. Davies and C. W. Jones, *Angew. Chem., Int. Ed.*, 2015, **54**, 6470–6474.
10 S. Elgue, T. Aillet, K. Loubiere, A. Conte, O. Dechy-Cabaret, L. Prat, C. Horn, O. Lobet and S. Vallon, *Chem. Today*, 2015, **33**, 58–61.
11 D. Caramelli, J. M. Granda, S. H. M. Mehr, D. Cambié, A. B. Henson and L. Cronin, *ACS Cent. Sci.*, 2021, **7**, 1821–1830.
12 I. Holland and J. A. Davies, *Front. Bioeng. Biotechnol.*, 2020, **8**, 571777.
13 J. M. Granda, L. Donina, V. Dragone, D.-L. Long and L. Cronin, *Nature*, 2018, **559**, 377–381.
14 P. J. Kitson, S. Glatzel and L. Cronin, *Beilstein J. Org. Chem.*, 2016, **12**, 2776–2783.
15 A. M. K. Nambiar, C. P. Breen, T. Hart, T. Kulesza, T. F. Jamison and K. F. Jensen, *ACS Cent. Sci.*, 2022, **8**, 825–836.
16 T. Hardwick and N. Ahmed, *Chem. Sci.*, 2020, **11**, 11973–11988.
17 S. Steiner, J. Wolf, S. Glatzel, A. Andreou, J. M. Granda, G. Keenan, T. Hinkley, G. Aragon-Camarasa, P. J. Kitson, D. Angelone and L. Cronin, *Science*, 2019, **363**, eaav2211.
18 M. W. Bordo, R. Oketokoun, C. J. Cross, K. Bao, J. H. Lee, I. Feygin, A. B. Chang, J. V. Frangioni and H. S. Choi, *ACS Comb. Sci.*, 2015, **17**, 303–309.
19 O. J. Plante, E. R. Palmacci and P. H. Seeberger, *Science*, 2001, **291**, 1523–1527.
20 L. Van Hijfte, G. Marciniak and N. Froloff, *J. Chromatogr. B: Biomed. Sci. Appl.*, 1999, **725**, 3–15.
21 P.-P. Yang, Y.-J. Li, Y. Cao, L. Zhang, J.-Q. Wang, Z. Lai, K. Zhang, D. Shorty, W. Xiao, H. Cao, L. Wang, H. Wang, R. Liu and K. S. Lam, *Nat. Commun.*, 2021, **12**, 4494.
22 S. Hyun, N. Park, S. H. Nam, D. H. Cheon, Y. Lee, H.-S. Lim and J. Yu, *Chem. Commun.*, 2021, **57**, 2388–2391.
23 G. Comellas, Z. Kaczmarska, T. Tarrago, M. Teixido and E. Giralt, *PLoS One*, 2009, **4**, e6222.
24 P. A. Clemons, A. N. Koehler, B. K. Wagner, T. G. Sprigings, D. R. Spring, R. W. King, S. L. Schreiber and M. A. Foley, *Chem. Biol.*, 2001, **8**, 1183–1195.
25 H. E. Blackwell, L. Perez, R. A. Stavenger, J. A. Tallarico, E. Cope Eatough, M. A. Foley and S. L. Schreiber, *Chem. Biol.*, 2001, **8**, 1167–1182.
26 M. Lebl, V. Krchnak, N. F. Sepetov, B. Seligmann, P. Strop, S. Felder and K. S. Lam, *Biopolymers*, 1995, **37**, 177–198.
27 S. J. Lee, S. J. Oh, W. Y. Moon, M. S. Choi, J. S. Kim, D. Y. Chi, D. H. Moon and J. S. Ryu, *Nucl. Med. Biol.*, 2011, **38**, 593–597.
28 A. Hutinec, R. Rupcic, D. Ziher, K. S. Smith, W. Milhous, W. Ellis, C. Ohrt and Z. I. Schonfeld, *Bioorg. Med. Chem.*, 2011, **19**, 1692–1701.
29 N. W. Hird, *Drug Discovery Today*, 1999, **4**, 265–274.
30 N. Hayashi, T. Sugawara, M. Shintani and S. Kato, *J. Autom. Chem.*, 1989, **11**, 212–220.
31 J. H. Lee, K. Bao, J. V. Frangioni and H. S. Choi, *Microarrays*, 2015, **4**, 53–63.
32 J. H. Lee, S. Park, H. Hyun, M. W. Bordo, R. Oketokoun, K. A. Nasr, J. V. Frangioni and H. S. Choi, *Anal. Chem.*, 2013, **85**, 3508–3514.
33 J. H. Lee, H. Hyun, C. J. Cross, M. Henary, K. A. Nasr, R. Oketokoun, H. S. Choi and J. V. Frangioni, *Adv. Funct. Mater.*, 2012, **22**, 872–878.
34 J. H. Lee, H. S. Choi, K. A. Nasr, M. Ha, Y. Kim and J. V. Frangioni, *Anal. Chem.*, 2011, **83**, 5283–5289.
35 S. Burke and G. D. Shorten, *Biochem. Soc. Trans.*, 2009, **37**, 318–322.
36 J. T. Nguyen, Y. Ashitate, I. A. Buchanan, A. M. Ibrahim, S. Gioux, P. P. Patel, J. V. Frangioni and B. T. Lee, *J. Surg. Res.*, 2012, **177**, e83–e88.
37 W. A. Macrae, *Br. J. Anaesth.*, 2008, **101**, 77–86.
38 E. Eisenberg, *Pain*, 2004, **111**, 3–7.
39 I. K. Crombie, H. T. Davies and W. A. Macrae, *Pain*, 1998, **76**, 167–171.
40 E. A. Owens, S. Lee, J. Choi, M. Henary and H. S. Choi, *Wiley Interdiscip. Rev.: Nanomed. Nanobiotechnol.*, 2015, **7**, 828–838.
41 S. L. Gibbs, Y. Xie, H. L. Goodwill, K. A. Nasr, Y. Ashitate, V. J. Madigan, T. M. Siclovan, M. Zavodszky, C. A. Tan Hehir and J. V. Frangioni, *PLoS One*, 2013, **8**, e73493.
42 H. Hyun, M. W. Bordo, K. Nasr, D. Feith, J. H. Lee, S. H. Kim, Y. Ashitate, L. A. Moffitt, M. Rosenberg, M. Henary, H. S. Choi and J. V. Frangioni, *Contrast Media Mol. Imaging*, 2012, **7**, 516–524.
43 A. Bajaj, N. E. LaPlante, V. E. Cotero, K. M. Fish, R. M. Bjerke, T. Siclovan and C. A. Tan Hehir, *J. Histochem. Cytochem.*, 2013, **61**, 19–30.

44 C. W. Barth and S. L. Gibbs, *Proc. SPIE-Int. Soc. Opt. Eng.*, 2016, **9696**, 96960R.
45 M. H. Park, H. Hyun, Y. Ashitate, H. Wada, G. Park, J. H. Lee, C. Njiojob, M. Henary, J. V. Frangioni and H. S. Choi, *Theranostics*, 2014, **4**, 823–833.
46 H. L. Morgan, *J. Chem. Doc.*, 1965, **5**, 107–113.
47 L. McInnes, J. Healy and J. Melville, arXiv, arXiv:1802.03426, 2018, preprint.
48 V. C. Tonn and C. Meier, *Chemistry*, 2011, **17**, 9832–9842.
49 A. T. Merritt, *Comb. Chem. High Throughput Screening*, 1998, **1**, 57–72.
50 L. Peng, R. Liu, J. Marik, X. Wang, Y. Takada and K. S. Lam, *Nat. Chem. Biol.*, 2006, **2**, 381–389.
51 V. V. Komnatnyy, T. E. Nielsen and K. Qvortrup, *Chem. Commun.*, 2018, **54**, 6759–6771.